Proceedings of the CAS–CERN Accelerator School: Free Electron Lasers and Energy Recovery Linacs, Hamburg, Germany, 31 May–10 June 2016, edited by R. Bailey, CERN Yellow Reports: School Proceedings, Vol. 1/2018, CERN-2018-001-SP (CERN, Geneva, 2018)

# Transverse Beam Dynamics

*B.J. Holzer*
CERN, Geneva, Switzerland

**Abstract**
This paper gives an overview of the transverse dynamics in particle accelerators. The main emphasis is on giving an introduction to the basic concepts, described in linear approximation, and allowing the reader to deduce the main parameters of a machine, based on some simple scaling laws.

**Keywords**
Accelerator physics; transverse dynamics.

## 1 Introduction

We would like to start this little essay with some kind of definition of 'what we are talking about' when we mention transverse beam dynamics. While the middle term, *beam*, might be clear enough, *transverse* and *dynamics* deserve some clarification. So in a desperate attempt to summarize in a few lines the key issues of this paper, we formulate the following questions. What do the particles do, while they are travelling along a linac or while we accelerate them in a circular machine? How do we manage to keep them on – or close to – a trajectory in a linear accelerator (even a linear collider in some cases) with deviations from this ideal path of only a fraction of a millimetre? How do we manage to convince our particle ensemble to travel distances that, in a storage ring, turn after turn, easily sum up to many millions of kilometres, without being lost?

Before we start to answer these questions, we would like to emphasize that we have to act with caution. We will use a language that has been developed for 'periodic structures', i.e. where the situation seen by the particle repeats itself after a certain time or distance. The reason lies at the bottom of the mathematics involved. Now, while this is easily fulfilled in a circular accelerator, namely in the case of a synchrotron, a linear accelerator does not have such a built-in periodicity: the particles pass through the machine only once and that's it. However, we like to make use of the expressions derived for the periodic machines, as they present a powerful and elegant tool to design the accelerator as well as to express the most relevant beam parameters. But in doing so we have to exercise due care. In the following sections, we will therefore describe this language and – wherever needed – make a clear point when we have to be careful and make a distinction between linacs and circular machines.

For the time being, let us state that an accelerator usually needs:

- a system of magnetic fields that create focusing forces to keep the particles together, and that ultimately lead to a well-defined beam size;
- in the case of a circular machine, magnetic bending fields to keep the particles on a closed, more or less circular orbit;
- a mechanism to lock these $B$-fields to the changing particle energy and thus keep the particles on, or close to, this design orbit over the complete energy range of the machine;
- if the particles are successfully kept in both transverse planes, we need a radio frequency (RF) structure to accelerate the particles and create the necessary energy gain via longitudinal electric fields.

By definition of the title, we will neglect the last item in this paper. Here we just assume that our colleagues from the RF systems will do a good job. Those who are interested in the longitudinal



https://doi.org/10.23730/CYRSP-2018-001.145

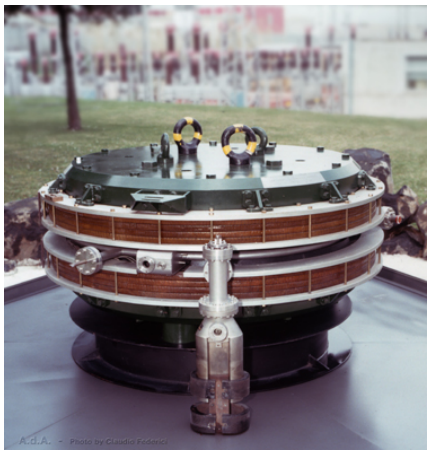

**Fig. 1:** Annelli de Accumulatione; the first electron–positron collider ring

**Fig. 2:** The tunnel of the LHC proton–proton collider at CERN, Geneva

dynamics are cordially invited to have a look at two brilliant papers, [1], [2]. For the time being we can concentrate on the issues related with the focusing properties of our accelerator.

So much for the definition. As the basic tools and so the language were developed for circular machines – synchrotrons in most cases – we will follow for a moment this concept, and further along the line we will include in our contemplations linear accelerators and transfer lines.

Two examples of synchrotrons to start with: the Annelli de Accumulatione (Fig. 1), as far as we know, the very first particle collider and certainly one of the smallest synchrotrons, built in Frascati by Bruno Touschek in 1944 [3]; and the large hadron collider (LHC) [4], at present the largest storage ring ever built, running at the highest achievable particle energies at CERN (Figs. 2 and 3).

## 2 Transverse beam dynamics

The transverse beam dynamics of charged particles in an accelerator describes the movement of single particles under the influence of the external transverse bending and focusing fields. It includes the detailed arrangement (for example, their positions in the machine and their strength) of the accelerator magnets used to obtain well-defined, predictable parameters of the stored particle beam, and it describes methods to optimize the trajectories of single particles, as well as the dimensions of the beam, considered as an ensemble of many particles. A treatment of this field in full mathematical detail, including sophisticated lattice optimizations, such as the right choice of the basic lattice cells and the design of dispersion

**Fig. 3:** The LHC proton–proton collider

suppressors or chromaticity compensation schemes, is beyond of the scope of this overview. For further reading and for more detailed descriptions, we therefore refer to the more complete explanations in Refs. [5–7]. For the time being, we will just give a basic introduction into the topic and explain – more or less hand-waving – how the trick goes.

### 2.1 Geometry of the ring

In general, magnetic fields are used in circular accelerators to provide the bending force and to focus the particle beam. In principle, the use of electrostatic fields would also be possible, but at high momenta (i.e., if the particle velocity is close to the speed of light), magnetic fields are much more efficient. The force acting on the particles, the Lorentz force, is given by

$$\mathbf{F} = q \cdot (\mathbf{E} + \mathbf{v} \times \mathbf{B}) \,. \tag{1}$$

For high-energy particle beams, the velocity $\mathbf{v}$ is close to the speed of light and so represents a nice amplification factor whenever we apply a magnetic field. As a consequence, it is much more convenient to use magnetic fields for bending and focusing the particles.

Therefore, neglecting electric fields for the moment, we write the Lorentz force and the centrifugal force on the particle on its circular path as

$$F_{\text{Lorentz}} = e \cdot v \cdot B \,, \tag{2}$$

$$F_{\text{centrifugal}} = \frac{\gamma m_0 v^2}{\rho} \,. \tag{3}$$

Assuming an idealized homogeneous dipole magnet along the particle orbit, having pure vertical field lines, we define the condition for a perfect circular orbit as equality between these two forces. This yields the following condition for the idealized ring:

$$\frac{p}{e} = B \cdot \rho \,, \tag{4}$$

where we are referring to protons and have accordingly set $q = e$. This condition relates the so-called beam rigidity $B\rho$ to the momentum of a particle that can be carried in the storage ring, and it ultimately defines, for a given magnetic field of the dipole magnets, the size of the storage ring.

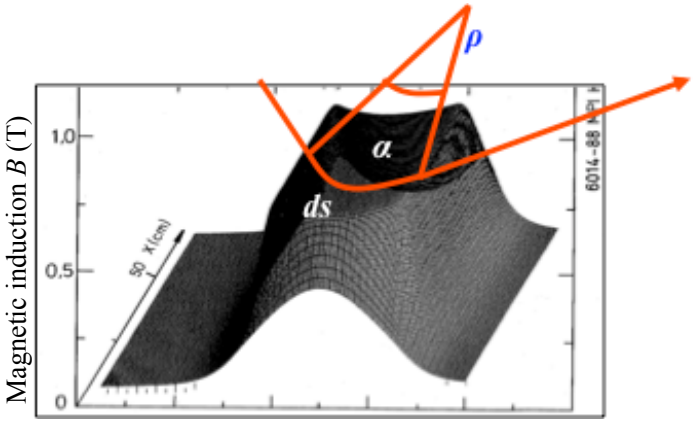


**Fig. 4:** Field map of a storage ring dipole magnet, and schematic path of a particle

In reality, instead of having a continuous dipole field, the storage ring will be built with several dipole magnets, powered in series to define the geometry of the ring. For a single magnet, the trajectory of a particle is shown schematically in Fig. 4. In the free space outside the dipole magnet, the particle trajectory follows a straight line. As soon as the particle enters the magnet, it is bent onto a circular path until it leaves the magnet at the other side.

The overall effect of the main bending (or 'dipole') magnets in the ring is to define this more or less circular path, which we call the 'design orbit'. By definition, this design orbit has to be a closed loop, and so the main dipole magnets in the ring have to define a full bending angle of exactly $2\pi$. If $\alpha$ denotes the bending angle of a single magnet, then

$$\alpha = \frac{\mathrm{d}s}{\rho} = \frac{B\,\mathrm{d}s}{B\cdot\rho}\,. \tag{5}$$

We therefore require that integrating over all dipole magnets we get

$$\frac{\int B\,\mathrm{d}s}{B\cdot\rho} = 2\pi\,. \tag{6}$$

Thus, a storage ring or synchrotron is not a 'ring' in the true sense of the word but more a polygon, where 'poly' means the discrete number of dipole magnets installed in the 'ring'.

In the case of the LHC, the dipole field has been pushed to the highest achievable values: 1232 superconducting dipole magnets, each 15 m long, define the geometry of the ring (or better 1232-gon, whatever the Greek expression for that might be) and thus, via Eq. (6), the maximum momentum for the stored proton beam. Using these equations, for a maximum momentum $p = 7$ TeV/$c$, we obtain a required magnetic field of

$$B = \frac{2\pi\cdot 7000\cdot 10^9\ \mathrm{eV}}{1232\cdot 14.3\ \mathrm{m}\cdot 2.99792\cdot 10^8\ \mathrm{m\,s^{-1}}}, \tag{7}$$

or

$$B = 8.33\ \mathrm{T}, \tag{8}$$

to bend the LHC beams. For convenience, we have expressed the particle momentum in units of GeV/$c$ here. Figure 5 shows a photograph of one of the LHC dipole magnets, built with superconducting NbTi filaments, which are operated at a temperature $T = 1.9$ K.

**Fig. 5:** Superconducting dipole magnet in the LHC storage ring

### 2.2 Focusing properties

In addition to the main bending magnets that guide the beam onto a closed orbit, focusing fields are needed to keep the particles close together. In modern storage rings and light sources, we have to keep more than $10^{12}$ particles in the machine, distributed over a number of bunches, and these particles have to be focused to keep their trajectories close to the design orbit. Furthermore, these particles are stored in the machine for many hours, and a carefully designed focusing structure is needed to maintain the necessary beam size at different locations in the ring and to guarantee stability of the transverse motion.

Following classical mechanics, linear restoring forces are used, just as in the case of a harmonic pendulum. Quadrupole magnets provide the corresponding field property: they create a magnetic field that depends linearly on the amplitude of the particle, i.e., the distance of the particle from the design orbit:

$$B_x = -g \cdot y\,, \qquad B_y = -g \cdot x\,. \tag{9}$$

The constant $g$ is called the gradient of the magnetic field and characterizes the focusing strength of the quadrupole lens in both transverse planes. The minus sign is a convention that follows the fact that for a positive amplitude, the field configuration of a focusing quadrupole will lead to a Lorentz force that reduces this amplitude, according to Fig. 6. As in the case of the dipole field, the quadrupole gradient is usually normalized to the particle momentum to obtain expressions that are valid for any particle momentum or energy. This normalized gradient is denoted by $k$ and defined as

$$k = \frac{g}{p/e} = \frac{g}{B\rho}\,. \tag{10}$$

The technical layout of such a quadrupole is depicted in Fig. 7. As in the case of the dipoles, the LHC quadrupole magnets were built using superconducting technology to achieve the highest possible focusing forces.

Now that we have defined the two basic building blocks of a storage ring, we need to arrange them in a so-called magnet lattice and optimize the field strengths in such a way as to obtain the required beam parameters. An example of such a magnet lattice is shown in Fig. 8. This photograph shows the dipole (orange) and quadrupole (red) magnets in the TSR storage ring in Heidelberg [8]. Eight dipoles are used to bend the beam into a 'circle', and the quadrupole lenses between them provide the focusing to keep the particles within the aperture limits of the vacuum chamber.

A general design principle of modern synchrotrons and storage rings should be pointed out here. In general, these machines are built following a so-called separate-function scheme: every magnet is

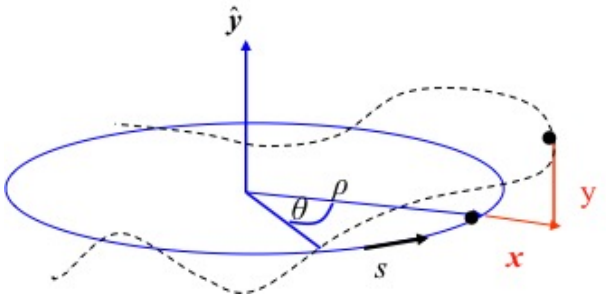


**Fig. 6:** Co-ordinate system used in particle beam dynamics: the longitudinal co-ordinate $s$ moves around the ring with the particle considered.

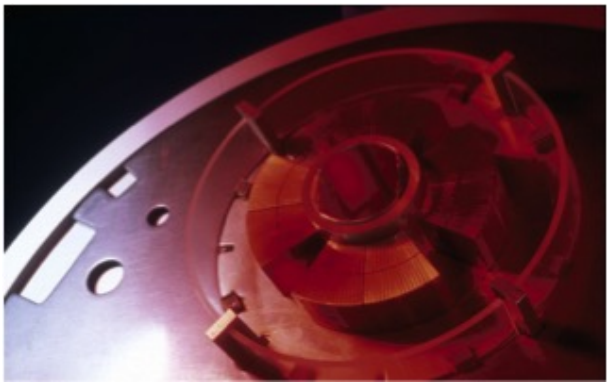

**Fig. 7:** Superconducting quadrupole magnet in the LHC storage ring

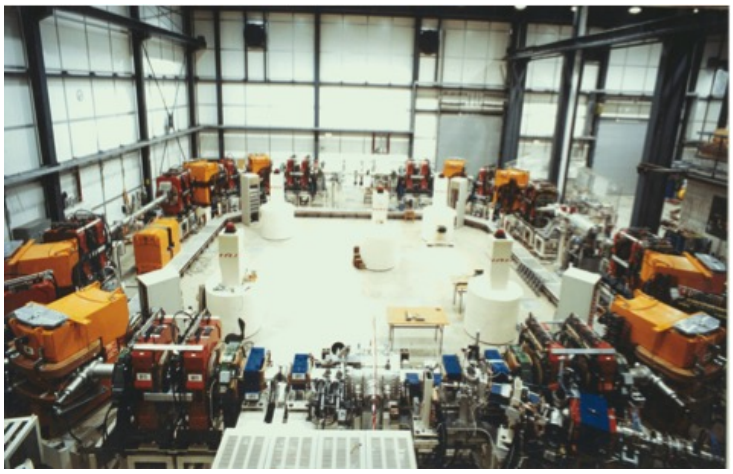

**Fig. 8:** The TSR storage ring, Heidelberg, is a typical example of a separate-function strong focusing storage ring [8].

designed and optimized for a certain task, such as bending, focusing, or chromatic correction. We separate the magnets in the design according to the job they are supposed to do; only in rare cases is a combined-function scheme chosen nowadays, where different magnet properties are combined in one piece of hardware. To express this principle mathematically, we use the general Taylor expansion of the normalized magnetic field,

$$\frac{B(x)}{p/e} = \frac{1}{\rho} + k \cdot x + \frac{1}{2!} m x^2 + \frac{1}{3!} n x^3 + \cdots . \tag{11}$$

Following these arguments, for the moment we take only constant (dipole-) or linear (quadrupole-) terms into account. The higher-order contributions to the field will be treated later as (hopefully) small perturbations.

Under these assumptions, we can derive – in linear approximation – the equation of motion of the transverse particle movement. We start with a general expression for the radial acceleration, known from classical mechanics (see, e.g., Ref. [9]):

$$a_r = \frac{\mathrm{d}^2\rho}{\mathrm{d}t^2} - \rho \left( \frac{\mathrm{d}\theta}{\mathrm{d}t} \right)^2 . \tag{12}$$

The first term refers to an explicit change in the bending radius, and the second to the centrifugal acceleration. Referring to our co-ordinate system, and replacing the ideal radius $\rho$ with $\rho + x$ for the general case (Fig. 6), we obtain the relation for the balance between the radial force and the counteracting Lorentz force:

$$F = m \frac{\mathrm{d}^2}{\mathrm{d}t^2}(x + \rho) - \frac{m v^2}{x + \rho} = e v B . \tag{13}$$

On the right-hand side of the equation, we take only linear terms of the magnetic field into account,

$$B_y = B_0 + x \frac{\mathrm{d}B_y}{\mathrm{d}x} , \tag{14}$$

and for convenience we replace the independent variable $t$ with the co-ordinate $s$,

$$x' = \frac{\mathrm{d}x}{\mathrm{d}s} = \frac{\mathrm{d}x}{\mathrm{d}t} \frac{\mathrm{d}t}{\mathrm{d}s} , \tag{15}$$

'Convenience' in this context means that we are more interested in the amplitude $x$ and angle $x'$ of the particle trajectory and therefore prefer the derivative of $x$ with respect to $s$. Thus, we obtain an expression for the particle trajectories under the influence of the focusing properties of the quadrupole and dipole fields in the ring, described by a differential equation. This equation is derived in its full beauty elsewhere [7], so we shall just state it here:

$$x'' - x \cdot \left( k - \frac{1}{\rho^2} \right) = 0 , \tag{16}$$

where $k$ is the normalized gradient introduced above and the $1/\rho^2$ term represents the so-called weak focusing, which is a property of the bending magnets. Depending on the actual sign of $k$, the quadrupole will focus (negative sign) or de-focus (positive sign) the beam in the corresponding plane. The situation is shown schematically in Fig. 6. An ideal particle will follow the design orbit represented by the circle in the diagram. Any other particle will perform transverse oscillations under the influence of the external focusing fields, and the amplitude of these oscillations will ultimately define the beam size. To be brief, and referring to the horizontal plane for a moment, we can make the statement that under the influence of the focusing fields from the quadrupoles $k$ and dipoles $1/\rho^2$, the transverse movement of the particles inside the single lattice elements looks like a harmonic oscillation.

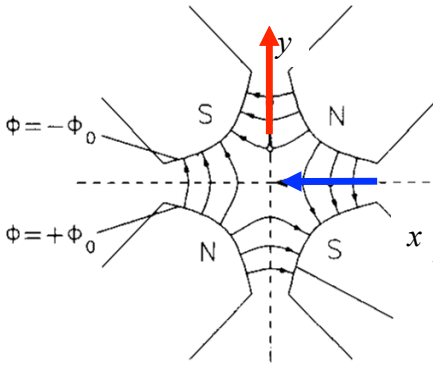


**Fig. 9:** Field configuration in a quadrupole magnet and the direction of the focusing and defocusing forces in the horizontal and vertical planes.

Unlike the case of a classical harmonic oscillator, however, the equations of motion in the horizontal and vertical planes differ somewhat. Assuming a horizontal focusing magnet, the equation of motion is as shown in Eq. (16). In the vertical plane, however, because of the orientation of the field lines and thus – in the end – by Maxwell's equations, the forces instead have a defocusing effect. Also, the weak focusing term disappears in general:

$$y'' + y \cdot k = 0\,. \tag{17}$$

The principal problem arising from the different directions of the Lorentz force in the two transverse planes of a quadrupole field is sketched in Fig. 9. As a consequence, to overcome this uncomfortable situation, we have to explicitly introduce quadrupole lenses that focus the beam in the horizontal and vertical directions in some alternating order. It is the task of the machine designer to find an adequate solution to this problem and to define a magnet pattern that will provide an overall focusing effect in both transverse planes. The rest is easy, in the sense of A. Wolski's statement: "...in principle, there are only two steps in the analysis of any dynamical system. The first step is to write down the equations of motion; and the second step is to solve them " [10].

Now, closely following the example of the classical harmonic oscillator, we can write down the solutions of the equations of motion. For simplicity, we focus on the horizontal plane; a 'focusing' magnet is therefore focusing in this horizontal plane and at the same time defocusing in the vertical plane. Starting with the initial conditions for the particle amplitude $x_0$ and angle $x_0'$ in front of the magnet element, we obtain the following relations for the trajectory inside the magnet:

$$x(s) = x_0 \cdot \cos\left(\sqrt{|K|}\,s\right) + x_0' \cdot \frac{1}{\sqrt{|K|}} \sin\left(\sqrt{|K|}\,s\right)\,, \tag{18}$$

$$x'(s) = -x_0 \cdot \sqrt{|K|} \sin\left(\sqrt{|K|}\,s\right) + x_0' \cdot \cos\left(\sqrt{|K|}\,s\right)\,. \tag{19}$$

Here, the parameter $K$ combines the quadrupole gradient and the weak focusing effect: $K := (1/\rho^2) - k$. Usually, these two equations are combined into a more elegant and convenient matrix form,

$$\begin{pmatrix} x \\ x' \end{pmatrix}_s = \mathbf{M}_{\text{foc}} \begin{pmatrix} x \\ x' \end{pmatrix}_0\,, \tag{20}$$

where the matrix $\mathbf{M}_{\text{foc}}$ contains all the relevant information about the magnet element:

$$\mathbf{M}_{\text{foc}} = \begin{pmatrix} \cos(\sqrt{|K|}\,s) & \frac{1}{\sqrt{|K|}} \sin(\sqrt{|K|}\,s) \\ -\sqrt{|K|} \sin(\sqrt{|K|}\,s) & \cos(\sqrt{|K|}\,s) \end{pmatrix}\,. \tag{21}$$

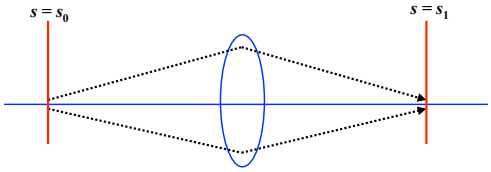


**Fig. 10:** Schematic illustration of the effect of a focusing quadrupole magnet

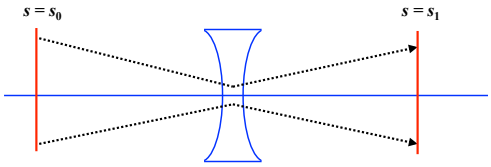


**Fig. 11:** Effect of a defocusing quadrupole magnet

The situation is illustrated in Fig. 10.

In the case of a defocusing magnet (or to be quite clear, also, in the case of the vertical plane, of a horizontal focusing magnet), we obtain analogously that

$$\begin{pmatrix} x \\ x' \end{pmatrix}_s = \mathbf{M}_{\text{defoc}} \begin{pmatrix} x \\ x' \end{pmatrix}_0 , \tag{22}$$

with

$$\mathbf{M}_{\text{defoc}} = \begin{pmatrix} \cosh(\sqrt{|K|}\, s) & \frac{1}{\sqrt{|K|}} \sinh(\sqrt{|K|}\, s) \\ \sqrt{|K|} \sinh(\sqrt{|K|}\, s) & \cosh(\sqrt{|K|}\, s) \end{pmatrix} ; \tag{23}$$

see Fig. 11.

For completeness, we also include the situation of field-free drift. In this trivial case with $K = 0$ we obtain

$$\mathbf{M}_{\text{drift}} = \begin{pmatrix} 1 & s \\ 0 & 1 \end{pmatrix} . \tag{24}$$

This matrix formalism allows us to combine the elements of a storage ring in an elegant way, and so it is straightforward to calculate particle trajectories. In this context, we would like to emphasize a few issues:

- a certain quadrupole lens will always have two opposing effects: focusing in one plane and defocusing in the other;
- et vice versa (and the other way round, for the non-Latin-speaking community);
- in linear approximation and without explicit coupling fields, such as roll angles of the quadrupoles or solenoids, the motion in the two transverse planes is uncoupled. An amplitude in the horizontal direction, e.g., will not have any influence on the vertical motion and therefore the corresponding non-diagonal elements of the matrix $M_{1,3}$, $M_{1,4}$, etc., are zero.
- It is therefore convenient to describe this simultaneous effect in the two planes in a single $4 \times 4$ matrix and define a vector for both transverse amplitudes and angles.

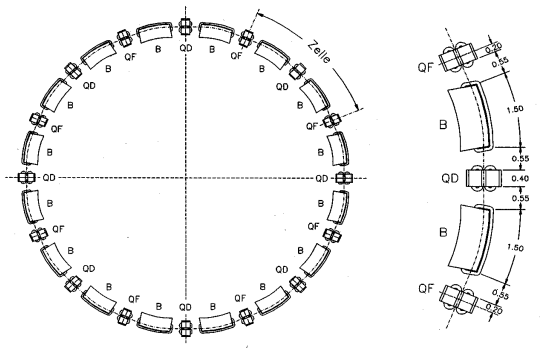


**Fig. 12:** A simple periodic chain of bending magnets (B) and focusing (QF) or defocusing (QD) quadrupoles forming the basic structure of a storage ring (court. [5]).

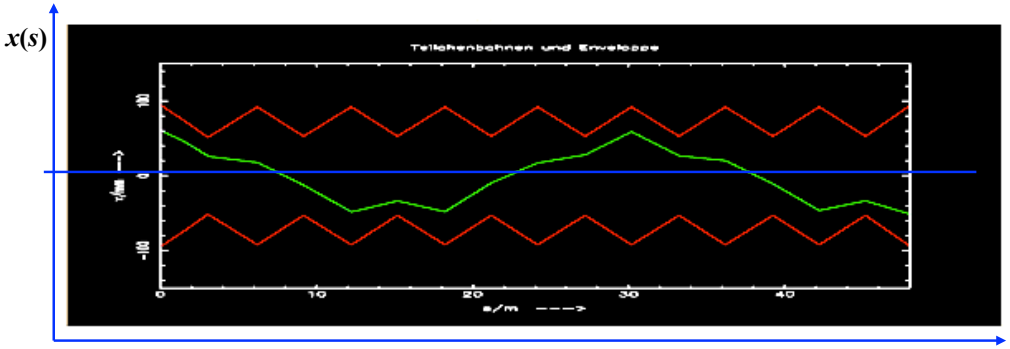


**Fig. 13:** Calculated particle trajectory in a simple storage ring

$$\begin{pmatrix} x \\ x' \\ y \\ y' \end{pmatrix}_s = \begin{pmatrix} \cos(\sqrt{|K|}\,s) & \frac{1}{\sqrt{|K|}}\sin(\sqrt{|K|}\,s) & 0 & 0 \\ -\sqrt{|K|}\sin(\sqrt{|K|}\,s) & \cos(\sqrt{|K|}\,s) & 0 & 0 \\ 0 & 0 & \cosh(\sqrt{|K|}\,s) & \frac{1}{\sqrt{|K|}}\sinh(\sqrt{|K|}\,s) \\ 0 & 0 & \sqrt{|K|}\sinh(\sqrt{|K|}\,s) & \cosh(\sqrt{|K|}\,s) \end{pmatrix} \cdot \begin{pmatrix} x \\ x' \\ y \\ y' \end{pmatrix}_0 . \tag{25}$$

As an example of a larger structure, we consider the simple case of an alternating focusing and defocusing lattice, a so-called FODO lattice [5]; see Fig. 12.

As we know the properties of each and every element in the accelerator, we can construct the corresponding matrices and calculate, step by step, the amplitude and angle of a single-particle trajectory around the ring. Even more conveniently, we can multiply out the different matrices and, given initial conditions $x_0$ and $x_0'$ at a certain position in the storage ring, directly obtain the trajectory at any location in the ring:

$$\mathbf{M}_{\text{total}} = \mathbf{M}_{\text{foc}} \cdot \mathbf{M}_{\text{drift}} \cdot \mathbf{M}_{\text{dipole}} \cdot \mathbf{M}_{\text{drift}} \cdot \mathbf{M}_{\text{defoc}} \cdots . \tag{26}$$

The trajectory thus obtained is shown schematically in Fig. 13.

We have to point out the following facts in this context.

– At each moment, which means inside each lattice element, the trajectory is a part of a harmonic oscillation.

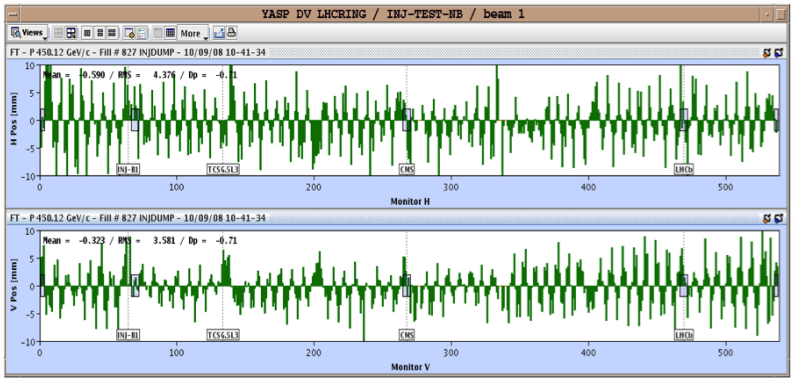


**Fig. 14:** Beam position measured in LHC on the first turn around the machine, during one of the very first beam injections into the LHC storage ring.

– However, because of the different restoring or defocusing forces, the solution will look different at each location.
– In the linear approximation that we have used in this context, all particles experience the same external fields, and their trajectories will differ only because of their different initial conditions.
– There seems to be an overall oscillation in both transverse planes while the particle is travelling around the ring. Its amplitude stays well within the boundaries set by the vacuum chamber, and its frequency in the example of Fig. 13 is roughly 1.4 transverse oscillations per revolution, which corresponds to the eigenfrequency of the particle under the influence of the external fields.

Coming closer to a real, existing machine, we see in Fig. 14 an orbit, measured during one of the first injections into the LHC storage ring. The horizontal oscillations are plotted in the upper half of the figure and the vertical oscillations in the lower half, on a scale of $\pm 10$ mm. Each histogram bar indicates the value recorded during the first turn of the beam by a beam position monitor at a certain location in the ring; the orbit oscillations are clearly visible. During these first injections, a beam screen had been introduced right after the injection point. In Fig. 15, the spot of the injected beam on this screen is clearly visible as well as the one after the first turn. In both transverse planes, these spots are not yet lying on top of each other and so the orbit is not yet closed. However, this can be achieved after a straightforward orbit correction and we finally obtain what we call a 'closed orbit'.

By counting (or, better, fitting) the number of oscillations in both transverse planes, we obtain, in the case of the LHC, values of

$$Q_x = 64.31\,, \qquad Q_y = 59.32\,. \tag{27}$$

These values, which describe the eigenfrequencies of the particles, are called the horizontal and vertical *tunes*, respectively. Knowing the revolution frequency, we can easily calculate the corresponding transverse oscillation frequencies, which for this type of machine usually lie in the range of several hundred kilohertz.

As the tune characterizes the particle oscillations under the influence of all external fields, it is one of the most important parameters of a storage ring. Therefore, it is usually displayed and controlled at all times by the control system of such a machine. As an example, Fig. 16 shows the tune diagram of the HERA proton ring [11]; this was obtained via a Fourier analysis of a spectrum measured from the signal of the complete particle ensemble. The peaks indicate the two tunes in the horizontal and vertical planes of the machine; in a sufficiently linear machine, a fairly narrow spectrum is obtained.

Briefly referring back to Fig. 13, the question is what the trajectory of the particle will look like in the second turn, or the third, or after an arbitrary number of turns. Now, as we are dealing with a circular

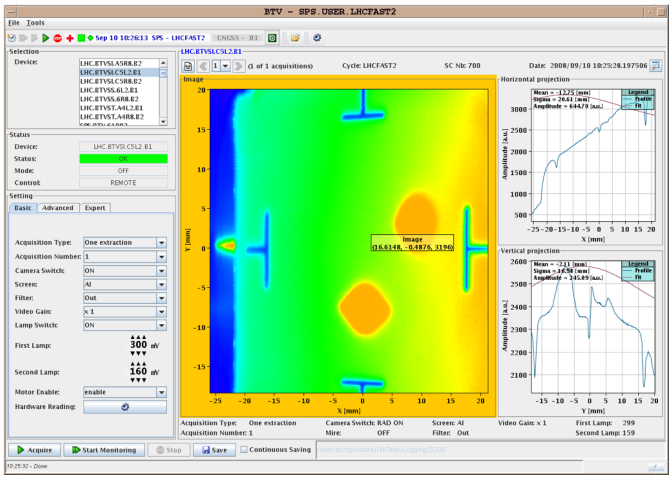

**Fig. 15:** Measured position of the first turn in LHC during the commissioning of the machine. The beam screen is located immediately after the injection septum and shows the spot at injection and after one full turn around the machine.

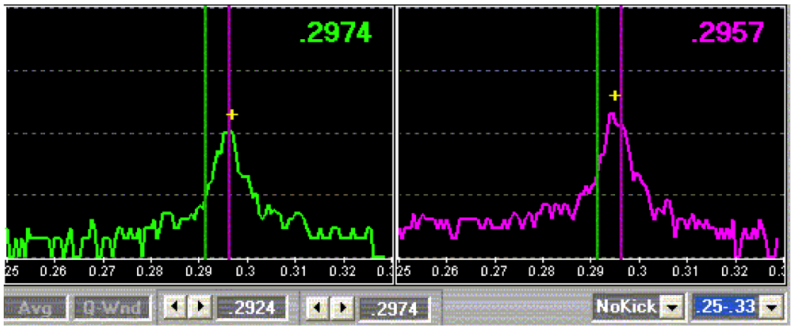


**Fig. 16:** Tune signal of a proton storage ring (HERA-p)

machine, the amplitude $x$ and angle $x'$ at the end of the first turn will be the initial conditions for the second turn, and so on. After many turns, the overlapping trajectories begin to form a pattern, such as that shown in Fig. 17, which indeed looks like a beam that here and there has a larger and a smaller size but still remains well defined in its amplitude by the external focusing forces.

## 3 The Twiss parameters $\alpha$, $\beta$, and $\gamma$

As explained in the last section, repeating the calculations that lead to the orbit of the first turn will result in a large number of single-particle trajectories that overlap in some way and form the beam envelope. Figure 17 shows the result for 50 turns. Clearly, as soon as we are talking about many turns or many particles, the use of the single-trajectory approach is quite limited and we need a description of the beam as an ensemble of many particles. Fortunately, in the case of periodic conditions in the accelerator, there is another way to describe the particle trajectories and, in many cases, it is more convenient than the aforementioned formalism. It is important to note that, in a circular accelerator, the focusing elements are necessarily periodic in the orbit co-ordinate $s$ after one revolution. Furthermore, storage ring lattices have an internal periodicity in most cases: they are often constructed, at least partly, from sequences in which identical magnetic structures, the lattice cells, are repeated several times in the ring and lead to periodically repeated focusing properties. In this case, the equation of motion can now be written in a

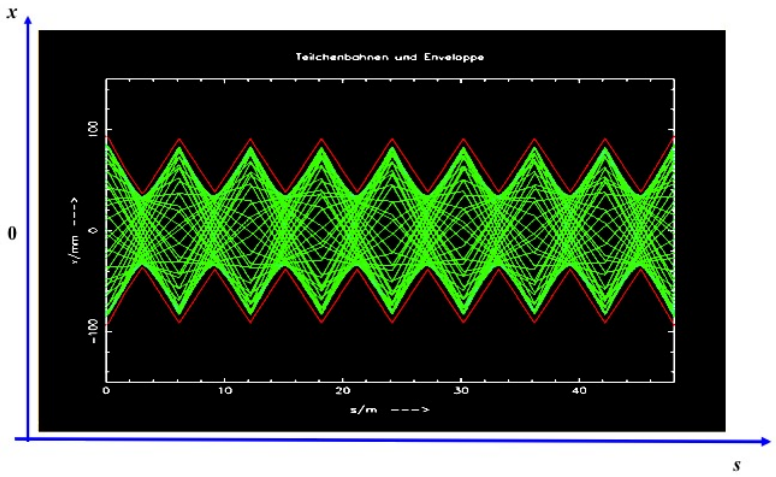


**Fig. 17:** Many single-particle trajectories together form a pattern that corresponds to the beam size in the ring

slightly different form:

$$x''(s) - k(s) \cdot x(s) = 0\,, \tag{28}$$

where, for simplicity, we refer to a pure quadrupole magnet and so the $1/\rho^2$ term does not appear. The main issue, however, is that unlike the previous treatment, the focusing parameters (or restoring forces) are no longer constant but are functions of the co-ordinate $s$. However, they are periodic in the sense that, at least after one full turn, they repeat themselves, i.e., $k(s + L) = k(s)$, leading to the so-called Hill differential equation. Following Floquet's theorem [6], the solution of this equation can be written in its general form as

$$x(s) = \sqrt{\varepsilon}\sqrt{\beta(s)}\cos(\psi(s) - \phi)\,, \tag{29}$$

where $\psi$ is the phase of the oscillation, $\phi$ is its initial condition, and $\varepsilon$ is a characteristic parameter of a single particle or, if we are considering a complete beam, of the ensemble of particles. Taking the derivative with respect to $s$, we get the trajectory angle $x'$:

$$x'(s) = \sqrt{\frac{\varepsilon}{\beta(s)}}\left(\frac{1}{2}\beta'(s)\cos\left(\psi(s) - \phi\right) - \sin(\psi(s) - \phi)\right)\,. \tag{30}$$

The position and angle of the transverse oscillation of a particle at a point $s$ are given by the value of a special amplitude function, the $\beta$-function, at that location; $\varepsilon$ and $\phi$ are constants of the particular trajectory. The $\beta$-function depends in a rather complicated manner on the overall focusing properties of the storage ring. It cannot be calculated directly by an analytical approach, but instead must be either determined numerically or deduced from properties of the single-element matrices (see, e.g., Ref. [7]). In any case, like the lattice itself, it must fulfil the periodicity condition

$$\beta(s + L) = \beta(s)\,. \tag{31}$$

Inserting the solution (Eq. (29)) into the Hill equation and rearranging slightly, we get

$$\psi(s) = \int_0^s \frac{\mathrm{d}s}{\beta(s)}\,, \tag{32}$$

which describes the phase advance of the oscillation. It should be emphasized that $\psi$ depends on the particle's oscillation amplitude. At locations where $\beta$ reaches large values, i.e., the beam has a large transverse dimension, the corresponding phase advance is small; conversely, at locations where we create

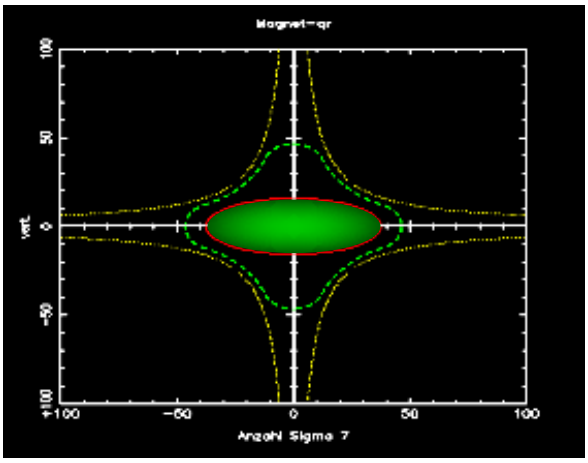


**Fig. 18:** Transverse beam shape inside a quadrupole magnet: plotted are $7\sigma$ of a Gaussian particle density distribution inside the vacuum chamber and magnet aperture.

a small $\beta$ in the lattice, we obtain a large phase advance. In the context of Fig. 13, we introduced the tune as the number of oscillations per turn, which is nothing else than the overall phase advance of the transverse oscillation per revolution in units of $2\pi$. So, by integrating Eq. (32) around the ring, we get, for the tune, the expression

$$Q = \frac{1}{2\pi} \oint \frac{\mathrm{d}s}{\beta(s)} \,. \tag{33}$$

The practical significance of the $\beta$-function is shown in Figs. 17 and 18. Whereas in Fig. 17 the single-particle trajectories are plotted turn by turn, Fig. 18 shows schematically a section through the transverse shape of the beam and indicates the beam size inside the vacuum chamber. The hyperbolic profile of the pole shoes of the quadrupole lens is sketched as a yellow dashed line, and the envelope of the overlapping trajectories, given by $\hat{x} = \sqrt{\varepsilon\beta(s)}$, is marked in red and is used to define the beam size in the sense of a Gaussian density distribution.

### 3.1 $\beta$, $\varepsilon$, and the phase space ellipses

Although the $\beta$-function is a somewhat abstract parameter that results from all focusing and defocusing elements in the ring, the integration constant $\varepsilon$ has a well-defined physical interpretation. Given the solution of Hill's equation, Eq. (29), and its derivative, Eq. (30), we can transform the first equation to

$$\cos\left(\psi(s)\right) = \frac{x(s)}{\sqrt{\varepsilon\beta(s)}} \tag{34}$$

and insert the expression into Eq. (30) to get an expression for the integration constant $\varepsilon$:

$$\varepsilon = \gamma(s)x^2(s) + 2\alpha x(s)x'(s) + \beta(s)x'^2(s) \,. \tag{35}$$

Here, we have followed the usual convention in the literature and introduced the two parameters

$$\alpha(s) = -\frac{1}{2}\beta'(s) \tag{36}$$

and

$$\gamma(s) = \frac{1+\alpha^2(s)}{\beta(s)} \,. \tag{37}$$

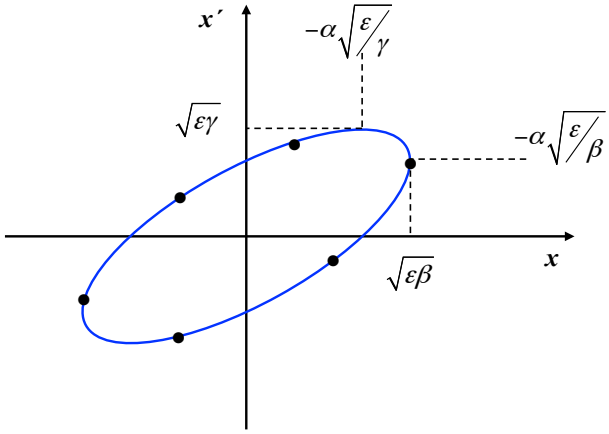


**Fig. 19:** Ellipse in $(x, x')$ phase space

We obtain for $\varepsilon$ a parametric representation of an ellipse in the $(x, x')$ 'phase space'. The mathematical integration constant thus gains physical meaning. In fact, $\varepsilon$ describes the space occupied by the particle in the transverse $(x, x')$ phase space (simplified here to a two-dimensional space). More specifically, the area in the $(x, x')$ space that is covered by the particle is given by

$$A = \pi \cdot \varepsilon \,, \tag{38}$$

and, as long as we consider only conservative forces acting on the particle, this area is constant according to Liouville's theorem. Here we take these facts as given, but we should point out that, as a direct consequence, the so-called emittance $\varepsilon$ cannot be influenced by any external fields; it is a property of the beam, and we have to take it as given and handle it with care.

To be more precise, and following the usual textbook treatment of accelerators, we can draw the ellipse of the particle's transverse motion in phase space; see, for example, Fig. 19. Although the shape and orientation are determined by the optics function $\beta$ and its derivative, $\alpha = -\frac{1}{2}\beta'$, and so change as a function of the position $s$, the area covered in phase space is constant.

In Fig. 19, expressions for the dependence of the beam size and divergence and, as a consequence, the shape and orientation of the phase space ellipse are included. For the sake of simplicity, we shall not derive these expressions here; instead, see Ref. [7].

Referring again to the single-particle trajectory (see Fig. 13), but now plotting the co-ordinates $x$ and $x'$ for a given position $s$ in the ring, turn by turn, we obtain the phase space co-ordinates of the particle as shown in Fig. 19 (marked as dots in the figure). These co-ordinates follow the form of an ellipse, whose shape and orientation are defined by the optical parameters at the reference position $s$ in the ring. Each point in Fig. 19 represents the transverse co-ordinates for a certain turn at that position in the ring, and the particle performs, from one turn to the next, a number of revolutions in phase space that corresponds to its tune. We have already emphasized that, as long as only conservative forces are considered (i.e., no interaction between the particles in a bunch, no collisions with remaining gas molecules, no radiation effects, etc.), the size of the ellipse in $(x, x')$ space is constant and can be considered as a quality factor of a single particle. Large areas in $(x, x')$ space mean large amplitudes and angles of transverse particle motion, and we would consider this as indicating a low particle 'quality'.

Let us now talk a little more about the beam as an ensemble of many (typically $10^{11}$) particles. Referring to Eq. (29), at a given position in the ring the single particle amplitude is defined by the emittance $\varepsilon$ and the function $\beta$. Thus, at a certain moment in time, the cosine term in Eq. (29) will be equal to one and the amplitude of the trajectory will reach its maximum value. Now, if we consider

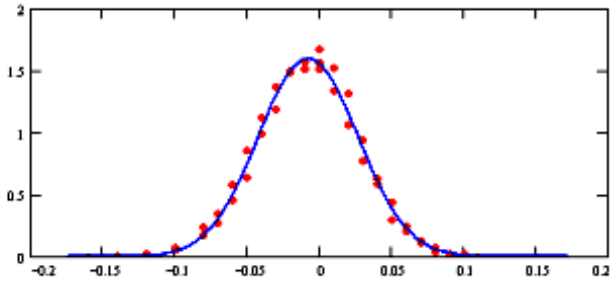


**Fig. 20:** Transverse particle distribution in a storage ring. The dots correspond to the measurement, the line is a Gaussian fit. A particle at $1\sigma$ from the beam centre is used to represent the beam size.

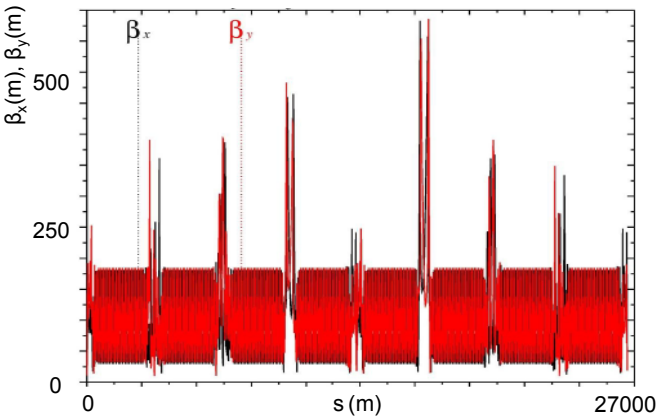


**Fig. 21:** LHC injection beam optics: owing to the larger beam emittance at low energy, the $\beta$-function has to be limited to values of about 600 m.

a particle at one standard deviation (sigma) of the transverse density distribution, then by using the emittance of this reference particle we can calculate the size of the complete beam, in the sense that the complete area (within one sigma) of all particles in the $(x, x')$ phase space is surrounded (and so defined) by our one-sigma candidate. Thus, the value $\sqrt{\varepsilon \cdot \beta(s)}$ defines the one-sigma beam size in the transverse plane.

An example of such a particle density distribution is shown in Fig. 20. The dots correspond to the measured values of the particle distribution at the collision point and the blue curve represents a Gaussian fit. The emittance (usually referred to as 'Courant – Snyder invariant') of the single particle at $1\sigma$ from the centre can be used as representative emittance of the beam ensemble.

It is the task of the lattice designer to establish a beam optics that guarantees – for a given emittance – values of the $\beta$-function that lead to tolerable beam sizes at every location in the machine. As an example, we shall use the values for the LHC proton beam (Fig. 21). In the periodic pattern of the arc, the $\beta$-function is equal to 180 m and the emittance $\varepsilon$ at the flat-top energy is roughly $5 \times 10^{-10}$ rad m. The resulting typical beam size is, therefore, 0.3 mm. Now, clearly, we would not design a vacuum aperture for the machine based on a one-sigma beam size; typically, an aperture requirement corresponding to $12\sigma$ is a good rule to guarantee a sufficient beam lifetime, allowing for tolerances arising from magnet misalignment, optics errors, orbit fluctuations, and operational flexibility. In Fig. 22, part of the LHC vacuum chamber is shown, including the beam screen used to protect the cold bore from synchrotron radiation; this corresponds to a minimum beam size of $18\sigma$.

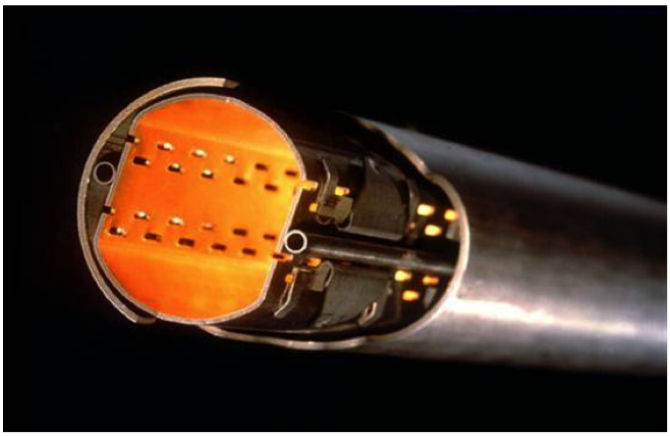

**Fig. 22:** LHC vacuum chamber with beam screen to shield the bore of the superconducting magnet from synchrotron radiation.

### 3.2 Adiabatic shrinking

The definition of the beam emittance described in the previous section bears a certain problem. Strictly speaking, Liouville's theorem states that – given conservative forces – the particle density in the phase space $x, p_x$ is constant. Now in accelerator physics we are talking about particle amplitudes and angles, $x, x'$ and a co-ordinate system defined by these variables is sometimes called the *trace space* to make a clear distinction from the *phase space*.

The main issue is related to the particle acceleration. The angle $x'$ of a particle is given by the ratio between longitudinal and transverse momentum:

$$x' = \frac{\mathrm{d}x}{\mathrm{d}s} = \frac{\mathrm{d}x}{\mathrm{d}t}\frac{\mathrm{d}t}{\mathrm{d}s} = \frac{p_x}{p_s} \propto \frac{1}{m_0 c\beta\gamma}\,, \tag{39}$$

where we express the relativistic momentum as a function of the rest mass $m_0$, and the relativistic parameters $\beta = v/c$ and the Lorentz factor $\gamma = \{1/\sqrt{(1-\beta^2)}\}$. $p_s$ describes the longitudinal component of the particle's momentum; and it is this longitudinal component that increases during the acceleration. Now, Liouville's theorem states that for the canonical conjugate variables $x$ and $p_x$ the phase space area is constant:

$$\int p_x \mathrm{d}x = \text{constant}\,, \tag{40}$$

and we will not argue about that.

However, in the rather sloppy interpretation that we have used until now, we refer to a co-ordinate system $x, x'$ and so in reality we get

$$\int x' \mathrm{d}x = \frac{\int p_x}{p_s} \mathrm{dx} \tag{41}$$

and as, during acceleration, the longitudinal momentum is obviously increasing, our $x$–$x'$ ellipse will shrink proportionally to $1/\beta\gamma$. We conclude, therefore, that the beam emittance and, as a consequence, the beam dimension in both transverse planes will shrink during acceleration and this is indeed what we observe. As a consequence, a proton beam in a synchrotron or an electron beam in a linac will have the largest emittance at injection energy and it is here, where the beam optics – expressed as a $\beta$-function – will have to be optimized for sufficient free aperture. The effect can be quite impressive: in Figs. 23 and 24, the $7\sigma$ envelope of a proton beam is shown inside the vacuum chamber (dashed line) of a mini-beta quadrupole magnet. Figure 23 shows the situation at 40 GeV injection energy. Figure 24 – for the same beam optics, and at the same location again – shows the $7\sigma$ envelope, but now at flat-top energy

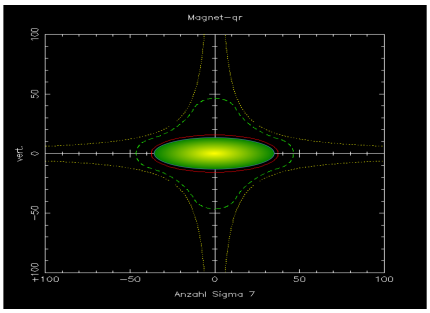


**Fig. 23:** Beam envelope of HERA proton ring at 40 GeV injection energy. The plot refers to $7\sigma$ at the mini-beta quadrupoles.

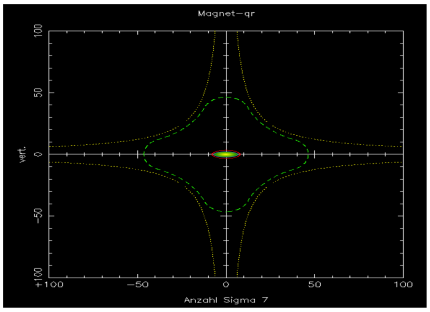


**Fig. 24:** Beam envelope of the HERA proton ring at 920 GeV flat-top energy. The plot refers to $7\sigma$ at the mini-beta quadrupoles.

of 920 GeV. Owing to the much higher energy, the beam size is smaller by a factor of $\sqrt{920/40}$ and the beam lifetime was considerably increased on the energy ramp of this machine.

As a direct consequence, we conclude that beam optics that lead to large beta functions in the ring only can be applied at highest energy, where, due to the reduced emittance, the overall beam size still can be limited. As an example, we refer again to the LHC situation. In direct comparison with the low-energy optics shown in Fig. 21, we now present the optics applied for high-energy collisions, Fig. 25. Here we can afford values of $\beta$ of up to 4.5 km.

For completeness, we have to mention that as soon as synchrotron light effects must be considered, the situation changes drastically. In electron synchrotrons, the beam dynamics is determined by the equilibrium between synchrotron radiation damping and excitation due to the emitted photon quanta. Therefore, in those cases, we observe a quadratic increase of the emittance with energy [14]

## 4 Errors in field and gradient

So far, we have treated the beam and the equation of motion as a mono-energetic problem. Unfortunately, in the case of a realistic beam, we have to deal with a considerable distribution of the particles with respect to energy or momentum. A typical value is

$$\frac{\Delta p}{p} \approx 1.0 \cdot 10^{-3} \,. \tag{42}$$

This momentum spread leads to several effects concerning the bending of the dipole magnets and the focusing strength of the quadrupoles. It turns out that the equation of motion, which has been a homogeneous differential equation until now, acquires a non-vanishing term on the right-hand side.

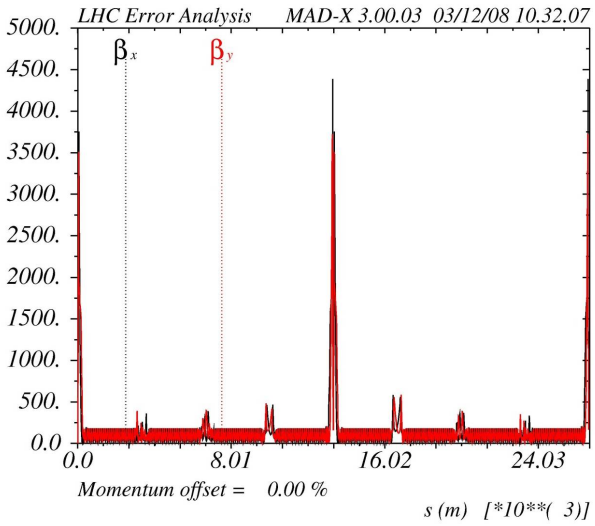


**Fig. 25:** LHC beam optics at high energy: Due to the small beam emittance at high energy, large values of the amplitude function $\beta$ can be accepted; to be compared with the situation at injection energy, Fig.21.

### 4.1 Dispersive effects

Replacing the ideal momentum $p$ in Eq. (10) with $p_0 + \Delta p$, we obtain in approximation of small $\Delta p$, instead of Eq. (16):

$$x'' + x \cdot \left( \frac{1}{\rho^2} - k \right) = \frac{\Delta p}{p_0} \cdot \frac{1}{\rho} \,. \tag{43}$$

The general solution of our now inhomogeneous differential equation is, therefore, the sum of the solution of the homogeneous equation of motion and a particular solution of the inhomogeneous equation:

$$x(s) = x_\beta(s) + x_\mathrm{i}(s) \,. \tag{44}$$

Here, $x_\beta$ is the solution that we have discussed up to now and $x_\mathrm{i}$ is an additional contribution that still has to be determined. For convenience, we usually normalize this second term and define a special function, the so-called dispersion:

$$D(s) = \frac{x_\mathrm{i}(s)}{\Delta p / p_0} \,. \tag{45}$$

This describes the dependence of the additional amplitude of the transverse oscillation on the momentum error of the particle. In other words, it fulfils the condition

$$x_\mathrm{i}''(s) + K(s) \cdot x_\mathrm{i}(s) = \frac{1}{\rho} \cdot \frac{\Delta p}{p_0} \,. \tag{46}$$

As before, we have combined the weak and strong focusing effects in the parameter $K := (1/\rho^2) - k$. The dispersion function is defined by the magnet lattice and is usually calculated by optics programs in the context of the calculation of the usual optical parameters. Analytically, it can be determined for single elements via the expression

$$D(s) = S(s) \cdot \int \frac{1}{\rho(\bar{s})} C(\bar{s}) \, \mathrm{d}\bar{s} - C(s) \cdot \int \frac{1}{\rho(\bar{s})} S(\bar{s}) \, \mathrm{d}\bar{s} \,, \tag{47}$$

where $S(s)$ and $C(s)$ correspond to the sine-like and cosine-like elements of the single-element matrices or of the corresponding product matrix if there are several elements considered in the lattice.

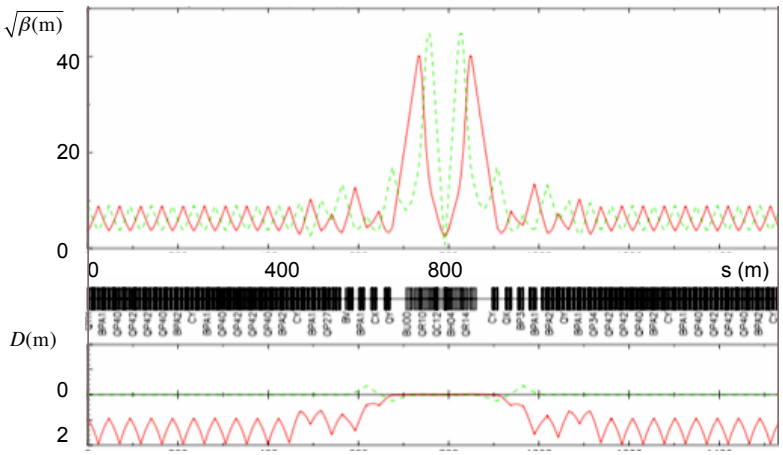


**Fig. 26:** $\beta$-function (top) and dispersion (bottom) of a typical high-energy collider ring

Although this all sounds somewhat theoretical, we would like to stress that typical values for the beam size and dispersive effect in the case of a high-energy storage ring are

$$x_\beta \approx 1\text{–}2 \text{ mm}\,, \qquad\qquad D(s) \approx 1\text{–}2 \text{ m}\,. \tag{48}$$

Thus, for a typical momentum spread of $\Delta p/p = 1 \cdot 10^{-3}$, we obtain an additional contribution to the beam size from the dispersion function that is of the same order as that from the betatron oscillations, $x_\beta$. An example of a high-energy beam optics system including the dispersion function is shown in Fig. 26. It should be pointed out that the dispersion describes the special orbit that an ideal particle would have in the absence of betatron oscillations ($x_\beta = x'_\beta = 0$) for a momentum deviation of $\Delta p/p = 1$. Nevertheless, it describes 'just another particle orbit' and so it is subject to the focusing forces of the lattice elements, as seen in the figure.

### 4.2 Chromaticity

Whereas dispersion is a problem that describes the non-ideal bending effect of dipoles for the case of a momentum error (or spread) in the particles, the careful reader will not be surprised to learn that a similar effect exists for the quadrupole focusing. We call this *chromaticity*. The chromaticity $Q'$ describes an optical error of a quadrupole lens in an accelerator: for a given magnetic field, i.e., gradient of the quadrupole magnet, particles with a smaller momentum will feel a stronger focusing force, and particles with a larger momentum will feel a weaker force. The situation is shown schematically in Fig. 27. As a consequence, the tune of an individual particle will change, and the chromaticity $Q'$ relates the resulting tune shift to the relative momentum error of the particle. In linear approximation, we write

$$\Delta Q = Q' \cdot \frac{\Delta p}{p_0}\,. \tag{49}$$

$Q'$ is a consequence of the focusing properties of the quadrupole magnets and is thus given by the characteristics of the lattice. For small momentum errors $\Delta p/p_0$, the focusing parameter $k$ can be written as

$$k(p) = \frac{g}{p/e} = \frac{ge}{p_0 + \Delta p}\,, \tag{50}$$

where $g$ denotes the gradient of the quadrupole lens, $p_0$ the design momentum, and the term $\Delta p$ refers to the momentum error. If $\Delta p$ is small, as we have assumed, we can write in a first-order approximation,

$$k(p) \approx \frac{ge}{p_0}\left(1 - \frac{\Delta p}{p_0}\right)\,. \tag{51}$$

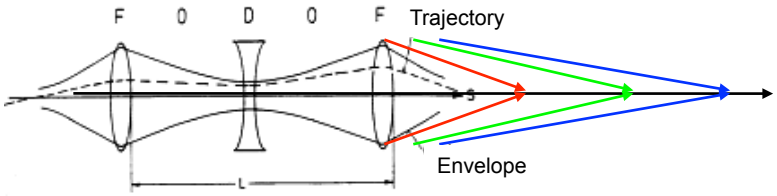


**Fig. 27:** Chromaticity effect in a quadrupole lens

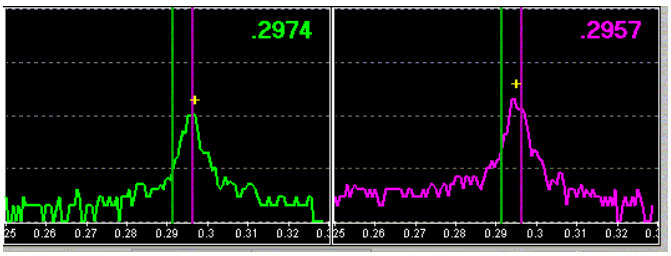


**Fig. 28:** Tune spectrum of a proton beam with a well-corrected chromaticity $Q' \approx 1$

This describes a quadrupole error

$$\Delta k = -k_0 \cdot \frac{\Delta p}{p}\,, \tag{52}$$

and so

$$\Delta Q = \frac{1}{4\pi} \int \Delta k\, \beta(s)\, \mathrm{d}s\,, \tag{53}$$

$$\Delta Q = -\frac{1}{4\pi} \frac{\Delta p}{p} \int k_0 \beta(s)\, \mathrm{d}s\,. \tag{54}$$

The negative sign indicates that a positive momentum deviation leads to a weaker focusing strength and, accordingly, to a lower tune. By definition, the linear chromaticity $Q'$ of a lattice is therefore given by

$$Q' = -\frac{1}{4\pi} \int k(s)\beta(s)\, \mathrm{d}s\,. \tag{55}$$

Now, unfortunately, although the dispersion created in the dipole magnets requires nothing more than some bigger aperture in the vacuum chamber, the chromaticity of the quadrupoles has an influence on the tune of the particles and so can lead to dangerous resonance conditions. Particles with a particular momentum error will be pushed into resonances and will be lost within a very short time. A look at the tune spectrum visualizes the problem. Whereas an ideal situation leads to a well-compensated chromaticity and the particles oscillate with basically the same frequency (Fig. 28), a non-corrected chromaticity ($Q'$ = 20 units in the case of Fig. 29) broadens the tune spectrum and a number of particles are pushed towards dangerous resonance lines.

In large synchrotrons, and storage rings in particular, this problem is crucial and represents one of the major factors that limit machine performance: because of the strong focusing of the quadrupoles and the large values of the $\beta-$function obtained, the chromaticity can reach considerable values. A chromaticity correction scheme is therefore indispensable. The trick goes in three steps.

– We sort the particles in the horizontal plane according to their momentum. This is done whenever we have a non-vanishing dispersion, for example, close to the focusing quadrupoles in the arc,

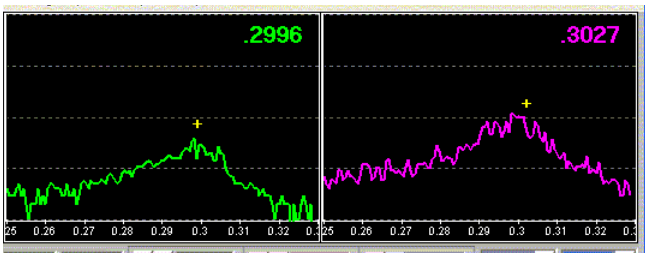


**Fig. 29:** Tune spectrum of a proton beam with a poorly matched chromaticity $Q' \approx 20$

where both the dispersion and the $\beta$-function reach high values and the particle trajectories are determined by the well-known relation $x_{\rm d}(s) = D(s) \cdot \Delta p/p$.

– At these places, we create magnetic fields that have a position-dependent focusing strength, in other words, fields that represent a position-dependent gradient. Sextupole magnets have exactly this property: if $g'$ describes the strength of the sextupole field, we get

$$B_x = g' \cdot xy \tag{56}$$

for the actual horizontal field component and

$$B_y = g' \frac{1}{2} \cdot (x^2 - y^2) \tag{57}$$

for the vertical component. The resulting effective gradient in both planes is obtained as

$$\frac{{\rm d}B_x}{{\rm d}y} = \frac{{\rm dB_y}}{{\rm d}x} = g' \cdot x\,. \tag{58}$$

– We now only have to adjust the strengths of two sextupole families (one each to compensate the horizontal and vertical chromaticities, respectively) to get an overall correction in both planes.

In a little more detail, and referring again to normalized gradients, we can write for the normalized quadrupole gradient of an off-centre particle in a sextupole magnet

$$k_{\rm sext} = \frac{e}{p} g' \cdot x_d = m \cdot x_d\,, \tag{59}$$

Here we have explicitly written $x_d$ to point out that it is the dispersive amplitude that is creating the position dependent quadrupole effect and so leads, for a given particle amplitude

$$x_{\rm d} = D \cdot \frac{\Delta p}{p}\,, \tag{60}$$

to the momentum-dependent focusing strength of the sextupole magnet:

$$k_{\rm sext} = m \cdot D \frac{\Delta p}{p}\,. \tag{61}$$

The combined effect of the so-called natural chromaticity created by the quadrupole lenses (Eq. (55)) and the compensation by the sextupoles leads to an overall chromaticity

$$Q' = -\frac{1}{4\pi} \oint (K(s) - m(s) \cdot D(s)) \beta(s)\, {\rm d}s \tag{62}$$

and needs to be compensated to zero in both transverse planes.

To summarize and make things as crystal clear as possible, the focusing properties of the magnet lattice lead to restoring forces in both transverse planes. The transverse motion of a particle is therefore a quasi-harmonic oscillation as the particle moves through the synchrotron, and the tune describes the frequency of these oscillations. As we cannot assume that all particles have exactly the same momentum, we have to take into account the effect of the momentum spread in the beam: the restoring forces are a function of the momentum of each individual particle and so the tune of each particle is different. We have to correct for this effect, and we do so by applying sextupole fields in regions where a non-vanishing dispersion distributes the off-momentum particles in the horizontal plane.

As easy as that!

## 5 Transformation of the Twiss parameters $\alpha, \beta, \gamma$

"Once more unto the breach, dear friends," [12].

While it is straightforward to develop the rules for transformation of the trajectory amplitudes and angles via the single-element matrices of the lattice elements, a similar formulation can be deduced for the optical functions $\alpha$, $\beta$, and $\gamma$. The derivation is closely related to the fact that – for a given energy – the beam emittance $\varepsilon$ is constant.

Starting from the usual transformation of a trajectory amplitude $x$ and angle $x'$ between two locations in the lattice

$$\begin{pmatrix} x \\ x' \end{pmatrix}_{s2} = \mathbf{M} \begin{pmatrix} x \\ x' \end{pmatrix}_{s1} , \tag{63}$$

where the matrix $\mathbf{M}$ describes the focusing properties of a single lattice element, or in case of several lattice elements, it represents the product matrix, as described in Eq. (26). In the general case of a sequence of lattice elements we write

$$\mathbf{M} = \begin{pmatrix} C & S \\ C' & S' \end{pmatrix} . \tag{64}$$

where the matrix elements $C, S, \ldots$ refer to the elements of the product matrix and in the trivial case of, e.g., a single focusing quadrupole are the usual descriptions that we introduced before:

$$\mathbf{M}_{\text{foc}} = \begin{pmatrix} C & S \\ C' & S' \end{pmatrix} = \begin{pmatrix} \cos(\sqrt{|K|}\, s) & \frac{1}{\sqrt{|K|}} \sin(\sqrt{|K|}\, s) \\ -\sqrt{|K|} \sin(\sqrt{|K|}\, s) & \cos(\sqrt{|K|}\, s) \end{pmatrix} . \tag{65}$$

Now we consider two locations $s_1$ and $s_2$ in the storage ring, as shown schematically in Fig. 30. At both positions, the emittance can be expressed as a function of the Twiss parameters at these positions:

$$\begin{aligned} \varepsilon &= \gamma_1 x^2(s1) + 2\alpha_1 x(s1) x'(s1) + \beta_1 x'^2(s1) , \\ \varepsilon &= \gamma_2 x^2(s2) + 2\alpha_2 x(s2) x'(s2) + \beta_2 x'^2(s2) , \end{aligned} \tag{66}$$

keeping in mind that the numerical value of the emittance at both positions has to be the same, as long as Mr. Liouville is fulfilled.

Knowing the amplitude and angle of the trajectory at position $s_2$, we can deduce these values at position $s_1$:

$$\begin{pmatrix} x \\ x' \end{pmatrix}_{s_1} = \mathbf{M}^{-1} \begin{pmatrix} x \\ x' \end{pmatrix}_{s_2} , \tag{67}$$

where the matrix from $s_2$ to $s_1$ is the inverse transformation matrix,

$$\mathbf{M}^{-1} = \begin{pmatrix} S' & -S \\ -C' & C \end{pmatrix} \tag{68}$$

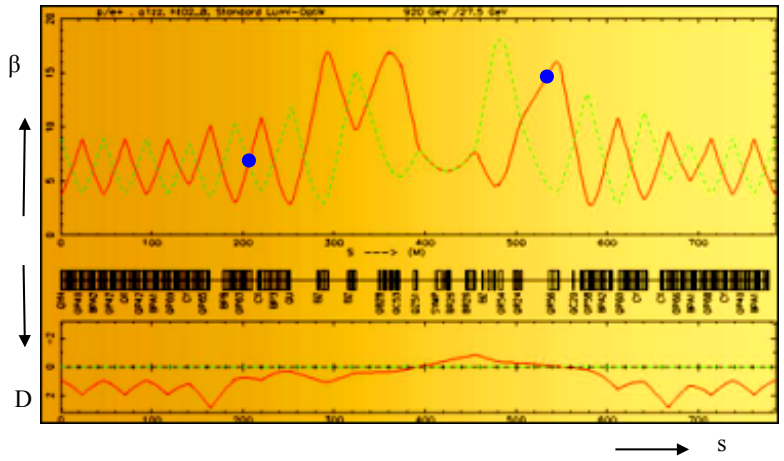


**Fig. 30:** The optical functions at two positions in a ring are related to each other via the constant beam emittance

and we used the fact that, for all matrices in a storage ring, the determinant has to be equal to one:

$$\det(M) = CS' - SC' = 1\,. \tag{69}$$

Thus, we can write for our trajectory co-ordinates:

$$x_1 = S'x_2 - Sx'_2\,, \tag{70}$$
$$x'_1 = -C'x_2 + Cx'_2\,. \tag{71}$$

Inserting these into Eq. (66), we express the emittance at position $s_1$ as a function of the trajectory co-ordinates at position $s_2$:

$$\varepsilon = \beta_1(Cx'_2 - C'x_2)^2 + 2\alpha_1(S'x_2 - Sx'_2)(Cx'_2 - C'x_2) + \gamma_1(S'x_2 - Sx'_2)^2\,. \tag{72}$$

Sorting via $x, x'$ and comparing the coefficients, we can finally relate the Twiss functions between the two locations in the ring:

$$\beta(s_2) = C^2\beta(s_1) - 2SC\alpha(s_1) + S^2\gamma(s_1) \tag{73}$$
$$\alpha(s_2) = -CC'\beta(s_1) + (SC' + S'C)\alpha(s_1) - SS'\gamma(s_1)\,, \tag{74}$$
$$\gamma(s_2) = C'^2\beta(s_1) - 2S'C'\alpha(s_1) + S'^2\gamma(s_1)\,. \tag{75}$$

Once more – for the sake of elegance in our notation – we prefer to combine these relations in matrix form and get

$$\begin{pmatrix}\beta\\ \alpha\\ \gamma\end{pmatrix}_{s_2} = \begin{pmatrix} C^2 & -2SC & S^2 \\ -CC' & SC' + CS' & -SS' \\ C'^2 & -2S'C' & S'^2 \end{pmatrix} \cdot \begin{pmatrix}\beta\\ \alpha\\ \gamma\end{pmatrix}_{s_1}\,. \tag{76}$$

So if we know by calculation or measurement the optical functions at one position in the ring, we can determine them via the single-element matrices in the lattice at any other location.

Now it is high time to handle the things with care: There is something special for transfer lines and linear accelerators that we have to mention and unfortunately it is a quite uncomfortable item: unlike rings, be they synchrotrons or storage rings, the optical functions $\alpha$, $\beta$, and $\gamma$ are not defined in

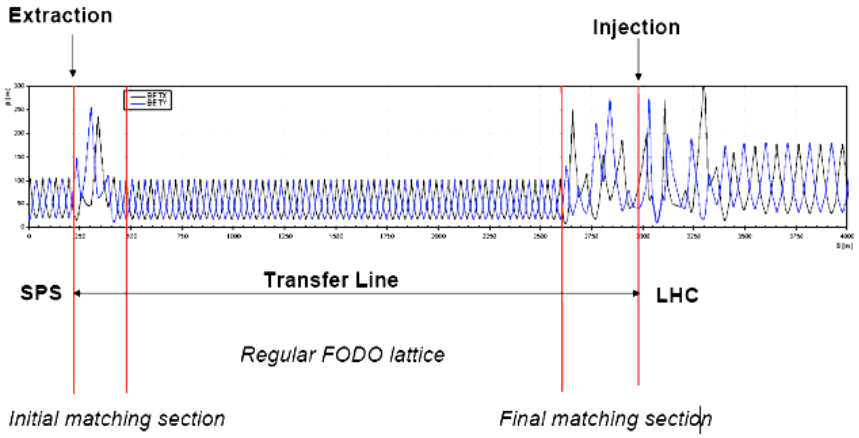


**Fig. 31:** Optics of the transfer line between the SPS and the HC


**Fig. 32:** The beam size must be measured at three locations in the transfer line

a non-periodic structure. Hill's equation requires a periodic system and so does its solution. Still, this description is very powerful and so our colleagues from the non-periodic world love to use our language. However, we should be aware of this issue. In Eq. (76) we have learnt how to transform the optical functions from one position in the lattice to another, knowing the focusing elements in between. This means that if we know, e.g., the Twiss functions at the beginning of a transfer line, we can calculate them through the complete linear structure. An example is given in Fig. 31.

In the case of the example in Fig. 31, the optical functions at the beginning of the structure are defined, i.e., uniquely determined by the periodicity of the SPS synchrotron. At the beginning and the end of the transfer line, special matching sections have been introduced to transform the periodic $\beta$-functions from the SPS lattice onto the transfer line structure and from here to the LHC cells. Usually, such a matching section leads for a moment to a somehow increased beam amplitude (due to the distorted $\beta$-functions) and we have to take care to limit the aperture needs to reasonable values.

More complicated, however, is the case, where a circular pre-accelerator does not exist. In such a case we have to 'guess' the initial values of $\alpha$, $\beta$, and $\gamma$, or, better, we have to measure them at the initial position before we can apply Eq. (76). To do so, we must perform three measurements at three different locations in the line (see Fig. 32) and obtain three values for the beam size:

$$\sigma_1 = \sqrt{(\varepsilon\beta_1)}$$
$$\sigma_2 = \sqrt{(\varepsilon\beta_2)}$$
$$\sigma_3 = \sqrt{(\varepsilon\beta_3)}$$

And this is the way the trick goes [13]:

Assume that we measure the particle distribution, which might look like the example in Fig. 33. Fitting a reasonable ellipse to the distribution, we can deduce the standard deviation of the, hopefully,

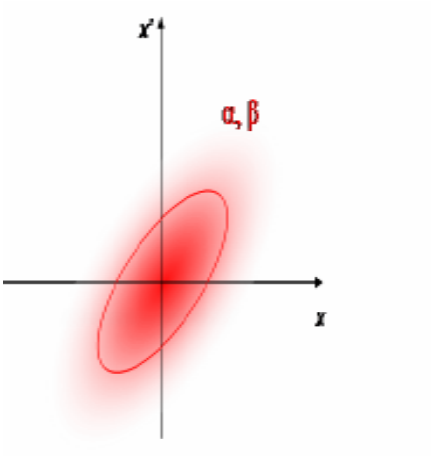


**Fig. 33:** Example of the transverse beam size measured in a transfer line

nicely Gaussian distributed particle density. (OK, for other than Gauss-distributions it will also work, more or less). So we obtain

$$\sigma = \sqrt{\varepsilon\beta} \tag{77}$$

and as the beam emittance is constant, we can write – referring to each of the three positions $s_0$, $s_1$, and $s_2$ –

$$\varepsilon = \frac{\sigma_0^2}{\beta_0} = \frac{\sigma_1^2}{\beta_1} = \frac{\sigma_2^2}{\beta_2}\,. \tag{78}$$

Now, from Eq. (76) we know how the $\beta$-functions transform through the lattice and so we can express $\beta_1$ and $\beta_2$ as a function of the initial value $\beta_0$:

$$\beta_1 = C_1^2\beta_0 - 2C_1S_1\alpha_0 + \frac{S_1^2}{\beta_0}\left(1+\alpha_0^2\right) \tag{79}$$

$$\beta_2 = C_2^2\beta_0 - 2C_2S_2\alpha_0 + \frac{S_2^2}{\beta_0}\left(1+\alpha_0^2\right)\,. \tag{80}$$

Using this information, we can determine both $\alpha_0$ and $\beta_0$:

$$\alpha_0 = \frac{1}{2}\beta_0\Gamma\,, \tag{81}$$

$$\beta_0 = \frac{1}{\sqrt{\left(\frac{\sigma_1}{\sigma_0}\right)^2/S_1^2 - \left(C_1/S_1\right)^2 + \left(C_1/S_1\right)\Gamma - \Gamma^2/4}}\,, \tag{82}$$

where we introduced the parameter

$$\Gamma = \frac{\left(\sigma_2/\sigma_0\right)^2/S_2^2 - \left(\sigma_1/\sigma_0\right)^2/S_1^2 - \left(C_2/S_2\right)^2 + \left(C_1/S_1\right)^2}{C_1/S_1 - C_2/S_2}\,.$$

## 6 Dipole errors and quadrupole misalignment

The design orbit, and thus the geometry of the ring or transfer line, is defined by the strength and arrangement of the dipole magnets. Under the influence of imperfections in the dipole field and (transverse) misalignment of the quadrupole magnets, unwanted deflection fields ('kicks') are created that influence

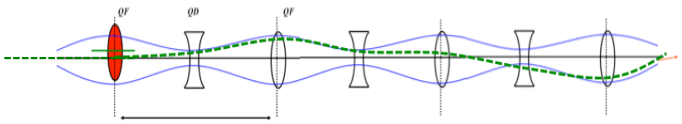

**Fig. 34:** Effect of a misaligned quadrupole in a transfer line

this orbit. If these distortions are small enough (and hopefully they are), we will still obtain an orbit that is not too far away from the design. It is this 'closed orbit' that acts as a reference for the single-particle trajectories and we have to take care that it does not differ too much from the design.

A special issue, however, arises from the fact that in a ring this reference orbit has, by definition, to be closed. While in a transfer line the effect of external distortions is somehow straightforward, in a periodic situation we have to be a bit more careful. A small field error $\delta B$ will result in a sudden change of the particle's angle $x'$ and so we describe the effect of a dipole error as

$$\Delta\theta = \Delta x' = \frac{\mathrm{d}l}{\rho} = \frac{\int \Delta B \mathrm{d}l}{B\rho}\,, \tag{83}$$

where we have again normalized the field error by the beam rigidity to obtain the deflection angle $x'$.

In a misaligned quadrupole, we get exactly the same problem. An offset $\Delta x$ in the presence of a field gradient $g$ leads to an effective dipole field that deflects the beam:

$$\Delta\theta = \frac{\int \Delta B \mathrm{d}l}{B\rho} = \frac{\int \Delta x g \mathrm{d}l}{B\rho}\,. \tag{84}$$

For a transfer line, the resulting effect is trivial. Assuming a short deflection, the amplitude $x$ of the particle is not affected by the field, but the angle $x'$ is and so we can write:

$$x_f = x_i = 0\,, \tag{85}$$

$$x'_f = x'_i + \Delta x' = x'_i + \frac{\int \Delta B \mathrm{d}l}{B\rho}\,. \tag{86}$$

From this moment on, the originally ideal trajectory will be transformed through the lattice elements in the usual way:

$$\begin{pmatrix} x \\ x' \end{pmatrix}_s = \mathbf{M} \begin{pmatrix} x \\ x' \end{pmatrix}_0\,, \tag{87}$$

which is shown qualitatively for a transfer line in Fig. 34.

In a circular machine, things get a bit more complicated. As we talk about a ring, the periodic boundary conditions after one turn have to be taken into account. Mathematically we express this fact by:

$$x(s+L) = x(s), \qquad x'(s+L) + \Delta x' = x'(s)\,. \tag{88}$$

While the orbit amplitude remains unchanged and the trajectory has to close upon itself, the angle $x'$ after one turn has to take the distortion $\mathrm{d}x'$ into account (Fig. 35). Starting from the general solution of Hill's equation, and using the periodicity condition we write for the amplitude

$$x(s) = a\sqrt{\beta(s)}\cos(\psi(s) - \phi)\,, \tag{89}$$

$$x(s+L) = x(s)\,, \tag{90}$$

$$a\sqrt{\beta(s+L)}\cos(\psi(s) + 2\pi Q - \phi) = a\sqrt{\beta(s)}\cos(\psi(s) - \phi)\,. \tag{91}$$


**Fig. 35:** Effect of a misaligned quadrupole in a ring: Following the periodicity condition, the orbit must close upon itself.

The amplitude factor $a$ will be determined later by the periodicity conditions and, clearly enough, the phase advance per turn increases by

$$\psi(s+L) = 2\pi Q\,.$$

As the amplitude function $\beta$ is periodic, by definition we obtain as first condition

$$\cos(2\pi Q - \phi) = \cos(-\phi) = \cos(\phi)\,, \tag{92}$$

$$\phi = \pi Q\,. \tag{93}$$

The boundary condition set by the amplitude fixes the initial condition for the phase $\phi$.

Following the same arguments, but now for the angle $x'$, we get

$$x(s) = a\sqrt{\beta(s)}\cos(\psi(s)-\phi)\,, \tag{94}$$

$$x'(s) = a\sqrt{\beta(s)}\,(-\sin(\psi(s)-\phi))\,\psi' + \frac{\beta'(s)}{2\sqrt{\beta}}a\cos(\psi(s)-\phi)\,, \tag{95}$$

and writing $\Delta x'$ for the local kick due to the field distortion

$$x'(s+L) + \Delta x' = x'(s) \tag{96}$$

we get

$$-a\frac{1}{\sqrt{\beta(\tilde{s}+L)}}\sin(2\pi Q-\phi) + \frac{\beta'(\tilde{s}+L)}{2\beta(\tilde{s}+L)}\sqrt{\beta(\tilde{s}+L)}a\cos(2\pi Q-\phi) + \delta x' = \\ -a\frac{1}{\sqrt{\beta(\tilde{s})}}\sin(-\phi) + \frac{\beta'(\tilde{s})}{2\beta(\tilde{s})}\sqrt{\beta(\tilde{s})}a\cos(-\phi)\,. \tag{97}$$

Here we have explicitly written $\tilde{s}$ for the position of the dipole field error, to emphasize, that, e.g., the optical functions are to be taken at this position. Knowing that, from the periodicity condition we derived,

$$\beta(s+L) = \beta(s), \qquad \phi = \pi Q\,, \tag{98}$$

we can solve for the amplitude $a$ and get

$$a = \delta x'\sqrt{\beta(\tilde{s})}\frac{1}{2\sin(\pi Q)}\,. \tag{99}$$

Inserting this equation into Eq. (89), we get the final result that the amplitude of the closed orbit under the influence of a dipole distortion (or quadrupole misalignment) is given by

$$x(s) = \delta x'\sqrt{\beta(\tilde{s})}\sqrt{\beta(s)}\frac{\cos(\psi(s)-\phi)}{2\sin(\pi Q)}\,. \tag{100}$$

We conclude that the distorted orbit depends on the kick strength, the local $\beta$-function at the location $\tilde{s}$ of the distortion, and the $\beta$-function at the observation point $s$. In addition, there is a resonance denominator,

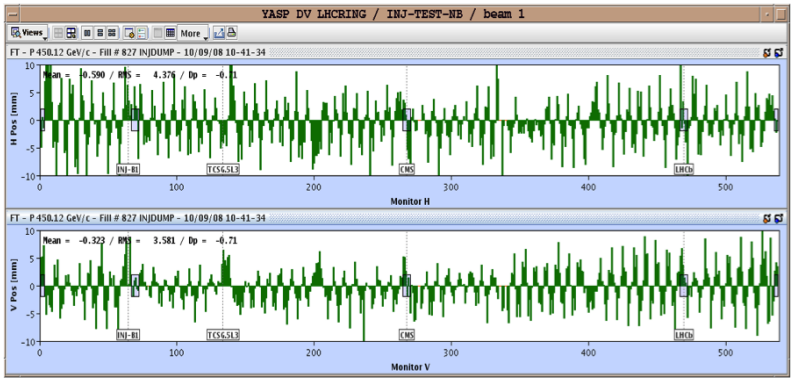


**Fig. 36:** Measured closed orbit in LHC during commissioning of the machine

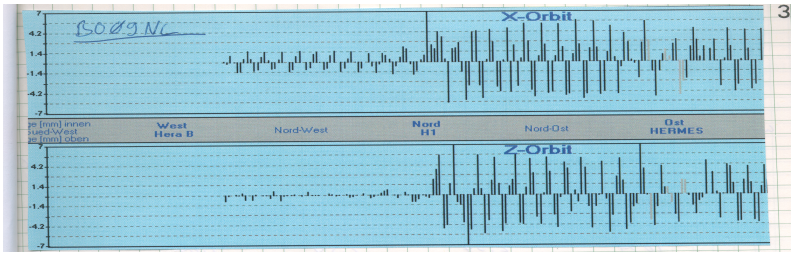


**Fig. 37:** Measured orbit in a beam transfer line, including the effect of a quadrupole lens that is misaligned in both planes. At the location of the misaligned magnet a sudden increase of the trajectory amplitude is observed .

which will amplify any external orbit distortion, if the tune in the corresponding plane is on, or close to an integer value. In such a case, the particle amplitude will grow ad infinitum and lead very quickly to particle losses; so better watch your tune!

For completeness: if we do not refer to a special starting point and express the orbit distortion as normalized dipole strength $\rho(\tilde{s})$, we get the general expression

$$x(s) = \frac{\sqrt{\beta(s)}}{2\sin(\pi Q)} \oint \sqrt{\beta(\tilde{s})}\frac{1}{\rho(\tilde{s})}\cos(|\psi(\tilde{s}) - \psi(s)| - \pi Q)\mathrm{d}\tilde{s}\,. \tag{101}$$

We would not like to close this section without showing a real example of orbits for both cases, a closed orbit in a storage ring and a real beam trajectory in transfer lines or linacs. We have seen an example of the first case already in Fig. 14, and we plot it here once more, for simplicity (Fig. 36). It shows the closed orbit of the LHC storage ring during the start-up phase of the machine, where considerable amplitudes in both planes were observed. The tune of the machine was set to $Q_x = 64.31$, so sufficiently away from resonance conditions. Still, the alignment tolerances of the magnets of $\Delta x \approx \Delta y \approx 150$ µm caused a considerable orbit distortion of up to 10 mm.

Figure 37 refers to the situation in a transfer line (observed at the HERA collider at DESY). While in the first part of the structure the oscillations are well corrected and small, suddenly a strong orbit fluctuation is created due to a misaligned quadrupole lens in the middle of the lattice. As the transfer line is, by definition, not closed upon itself, the observed orbit develops according to Eqs. (86) and (87).

### 6.1 Emittance in electron rings or linacs

There is a special issue about electron beams, that should not be forgotten: after all, they told us that this is an Accelerator School on electron machines. In Professor L. Rivkin's lecture [14], we heard that,

whenever we bend an electron beam, synchrotron radiation is emitted that has a strong influence on the beam dynamics. Summarizing briefly what we learnt there, we can state:

– The power of the radiated synchrotron light depends on the energy of the particle and the bending radius of the trajectory under the influence of the field acting on it,

$$\Delta P = \frac{e^2 c}{6\pi\varepsilon_0}\frac{\gamma^4}{\rho^2}\,. \tag{102}$$

– The energy loss per turn in a circular machine is given by

$$\Delta E = \frac{e^2}{3\varepsilon_0}\frac{\gamma^4}{\rho}\,. \tag{103}$$

– The critical energy of the emitted radiation is given by

$$\omega_{\rm c} = \frac{3c}{2}\frac{\gamma^3}{\rho}\,. \tag{104}$$

The damping effect of the light emission and the quantum effect of the emitted photons lead to an equilibrium emittance of the beam that is given by

$$\varepsilon_{x_0} = \frac{C_q E^2}{J_0}\frac{\langle H\rangle_{\rm mag}}{\rho}\,, \tag{105}$$

where $J_x$ is the so-called damping partition number, which is determined by the lattice and usually close to $J_x = 1$. The $H$-function describes the influence of the optical parameters $\alpha$, $\beta$, and $\gamma$ and the dispersion $D$.

$$\langle H\rangle = \gamma D^2 + 2\alpha D D' + \beta D'^2\,; \tag{106}$$

$C_q$ is a constant that we usually introduce to make our equations more compact. It is given by

$$C_q = \frac{55}{32\sqrt{3}}\frac{\hbar c}{(m_e c^2)^3}\,, \tag{107}$$

and for electrons it has the numerical value

$$C_q = 1.46810^{-6}\left[\frac{\rm m}{\rm GeV^2}\right]\,, \tag{108}$$

Now, while this all well known and clear and has a strong impact on the magnet strength and design of the lattice, it also affects the orbit correction scheme. Any (!) external field, including off-centre quadrupoles, and including the effect of orbit corrector dipoles, will influence the beam emittance. In the quest for smallest possible beam emittances, therefore, these effects must be taken into account.

Any deflecting field will change (i.e., create) additional beam emittance and we have to be careful when it comes to orbit corrections. Assume the two extreme cases, which are shown schematically in Figs. 38 and 39.

In the case of Fig. 38, the quadrupole magnets are slightly misaligned, leading to the orbit oscillations described above. The BPMs are assumed to be perfect and so they will show us how the real orbit looks like. Thus an orbit correction algorithm will calculate the most effective settings and tell us how to power our orbit correctors in a way to obtain a close-to-ideal orbit. Each misaligned quadrupole will lead to a orbit defection, which can and should be corrected by the corrector dipole next to it. The result will be a nearly perfect compensation of the quadrupole offsets and a nicely small beam emittance.

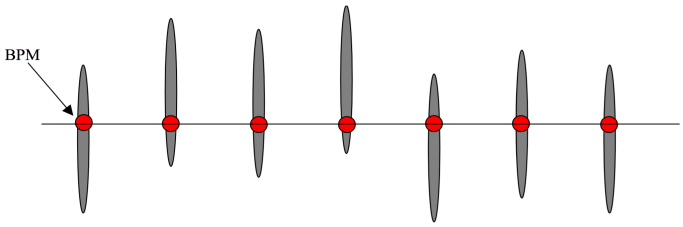


**Fig. 38:** Lattice with misaligned quadrupoles and perfect beam position monitors (BPMs)

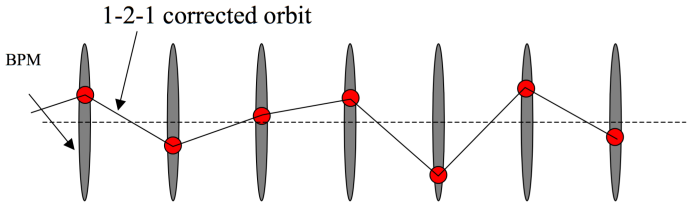


**Fig. 39:** Lattice with perfectly aligned quadrupoles but offsets in the reading of the beam position monitors (BPM). While the actual orbit is perfect, the beam position monitor readings simulate an orbit distortion.

Consider, however, the case of Fig. 39. Here the quadrupoles are exactly aligned, the orbit is perfect and it is the beam position monitor system that causes the trouble. Nobody is perfect and so even beam position monitors can have some reading errors that lead to artificial beam position offsets. A straightforward orbit correction approach, as explained, will reduce the beam position monitor readings, but in reality lead to a distorted orbit and so create additional dispersion in the machine and lead to increased emittances. In particular, in the vertical plane, this effect is most serious, as vertical bending fields will usually not be present in the machine and the emittance in this plane should be minimized. Special techniques are needed and have been developed to avoid such a problem. Dispersion-free steering methods are widely used [15, 16]; instead of naively correcting the orbit (i.e., the beam position monitor readings) we concentrate directly on the dispersion that can be measured in the machine and power our corrector magnets in such a way that the dispersion is minimized around the storage ring.

## References

[1] B.J. Holzer, in Proc. of the CAS-CERN Accelerator School, Erice, Italy, 24 April - 4 May 2013, CERN-2014-005 (CERN, Geneva, 2014), pp. 41-56. https://doi.org/10.5170/CERN-2014-005.41

[2] F. Tecker, in Proc. of the CAS-CERN Accelerator School, Trondheim, Norway, 18 - 29 August 2013, edited by W. Herr, CERN-2014-009 (CERN, Geneva, 2014), pp. 9-29. https://doi.org/10.5170/CERN-2014-009.9

[3] C. Bernardini, *Phys. Persp.* **6** (2004) 156. https://doi.org/10.1007/s00016-003-0202-y

[4] LHC design report Vol. 1: the LHC Main Ring, CERN-2004-003-V-1 (CERN, Geneva, 2004), https:/doi.org/10.5170/CERN-2004-003-V-1.

[5] K. Wille, *The Physics of Particle Accelerators* (Oxford University Press, Oxford, 2000).

[6] J. Rossbach and P. Schmüser, in Proc. of the CAS-CERN Accelarator School: 5th General Acceler-

ator Physics Course, Jyväskylä, Finland, 7–18 September 1992, edited by S. Turner, CERN-1994-001, (CERN, Geneva, 1994), pp. 17-88. https://doi.org/10.5170/CERN-1994-001.17

[7] B.J. Holzer, in Proc. of the CAS-CERN Accelerator School, Trondheim, Norway, 18 - 29 August 2013, edited by W. Herr, CERN-2014-009 (CERN, Geneva, 2014), pp. 61-100. https://doi.org/10.5170/CERN-2014-009.61

[8] E. Jaeschke *et al.*, The Heidelberg test storage ring for heavy ions TSR, Proc. EPAC, Rome, 1988, Ed. S. Tazzari (World Scientific, Teaneck, NJ, 1988), p. 365.

[9] H. Goldstein, *Klassische Mechanik* (Akademische Verlag-Gesellschaft, Wiesbaden, 1981).

[10] A. Wolski, *Beam Dynamics in High Energy Particle Accelerators* (Imperial College Press, London, 2014), p. 59. https://doi.org/10.1142/9781783262786-0002

[11] HERA Design Team, HERA: a proposal for a large electron proton colliding beam facility at DESY, DESY-HERA-81/10 (DESY, Hamburg, 1981).

[12] W. Shakespeare, *Henry V*, Act 3, Scene 1, Line 1.

[13] P.J. Bryant, in Proc. of the CAS-CERN Accelerator School, 5th General Accelerator Physics Course, Jyväskylä, Finland, 7–18 September 1992, CERN-1994-001 (CERN, Geneva, 1994), pp. 219-238. https://doi.org/10.5170/CERN-1994-001.17

[14] L. Rivkin, these proceedings

[15] T.O. Raubenheimer and R.D. Ruth, *Nucl. Instrum. Methods* **A302** (1991) 191. https://doi.org/10.1016/0168-9002(91)90403-D

[16] R. Assmann, *et al.*, Emittance optimization with dispersion free steering at LEP, CERN-SL-2000-078-OP, (CERN, Geneva, 2000).